# Massively Expanded NEA Accessibility via Microwave-Sintered Aerobrakes

Deep Space Industries Inc.

Phase 1 NIAC Report for
NNH16ZOA001N-17NIAC-A1

February 14, 2018

PI: John S. Lewis, Chief Scientist, Deep Space Industries

Co-I: Thomas T. Meek, Sr. Lecturer, Dept. of Materials Science & Engineering, University of Tennessee, Knoxville

Co-I: Christopher R. Cassell, Mission Planning, Deep Space Industries

# Table of Contents

# Massively Expanded NEA Accessibility via Microwave-Sintered Aerobrakes

## 1. Introduction

The availability of a wide range of natural resources among the near-Earth asteroid (NEA) population offers the opportunity to utilize these resources in the service of making access to most of the Solar System much easier than any classical approach which relies solely upon structural, heat-shield, life support and propellant materials lifted from Earth.

We have concentrated our attention on the two main factors that influence the application and utility of *in situ* aerobrake manufacture on near-earth asteroids. The first of these is the use of microwave sintering in the fabrication of aerocapture heatshields for retrieval of asteroidal materials into Earth orbit; the second is assessment of the performance of these aerocapture devices, including making very large numbers of NEAs accessible as sources of essential materials to support space exploration and exploitation.

The ability to provide propellants, life support materials, or structural metals in space is dependent upon identifying volatile-rich carbonaceous asteroids in orbits that are energetically accessible for outbound spacecraft. They must also be accessible for retrieval of returned material into Earth orbits that are well situated for launching such missions. The general NEA population is well suited to providing these materials; the subset of NEAs with the easiest access from (and to) Earth are the small population of bodies with heliocentric orbits that are closest to Earth and have the lowest orbital eccentricity (the Aten family). These bodies are generally quite small and faint, with diameters rarely larger than 100 meters. They also typically have long synodic periods of tens of years, which make both Earth-based astronomical studies and spacecraft launch opportunities infrequent and challenging.

As a result of these difficulties, Earth-based spectral characterization of these small bodies remains very incomplete; in the absence of spectral evidence for an economically attractive composition, there would be little incentive to launch exploratory spacecraft to such asteroids. These bodies also experience higher temperatures than most NEAs because they are

> 1) closer to the Sun,
>
> 2) are much smaller, and
>
> 3) have low-eccentricity orbits that do not provide lengthy "cold-soak" conditions near aphelion.

There is general reason to conclude that these bodies must have experienced more severe solar heating and outgassing than other NEAs with more typical (distant and eccentric) orbits. Even producing evidence for a significant population of dark (low albedo) bodies in near-Earth orbits would not demonstrate that they are attractive sources of volatiles; convincing proof that water is present would

require detection of the 3 µm water absorption feature, which requires such extreme sensitivity that tiny, faint, and rarely-visible asteroids would be unpromising observation targets. A compensatory benefit is that such bodies provide lower encounter velocities with Earth, so that capture into Earth orbit by a single lunar flyby is possible.

The broader population of NEAs, typically of much larger size, much larger aphelion distances (mostly Apollo asteroids), and with much shorter synodic periods, provides thousands of attractive targets that require larger return velocities. Many of these asteroids are kilometers in diameter and come with strong spectral data for the presence of water.

It is this expectation that the target asteroid masses and compositions will direct our attention to Apollo asteroids rather than Atens that makes it necessary (and profitable) to consider higher $v_\infty$ approaches to Earth. Approach velocities up to 5 km/s are considered in this report and would vastly increase the number of accessible NEAs. Such high approach velocities require a means of energy dissipation during capture that exceeds the ability of a lunar swingby to effect capture. Purely propulsive capture maneuvers become prohibitively expensive at such high approach velocities, suggesting aerobraking as an approach that minimizes propellant use and has the additional benefit of making the material of the used aerobrake available for processing in the target Earth orbit.

# 2. Fabrication of Aerobrakes on NEAs

## 1.1. Introduction

Success of this overall concept – returning volatiles and other materials from NEAs in less-than-Earthlike-orbits – requires minimizing the outbound mass because the target NEAs will generally have higher dV requirements than NEAs in Earthlike orbits. Fabricating the aerobrake required for capture into Earth orbit largely from lightly processed NEA regolith reduces outbound mass. Previous research on lunar soils indicated that microwave sintering of the regolith into a cohesive mass would require less energy than conventional thermal heating; this part of research subjected asteroid regolith simulants to both microwave and thermal heating to determine the energy savings of utilizing microwave sintering.

During this investigation, mechanical properties of a CI carbonaceous chondrite asteroid regolith were investigated using microwave and conventional heating. Properties such as flexure strength, Young's modulus of elasticity, and hardness as a function of porosity were determined. Fracture toughness, thermal shock, thermal conductivity, thermal diffusivity and sample density were also determined. Processing temperatures ranged from 1125 °C and 1300 °C with hold times of 15 and 30 minutes at peak temperature. The data suggests that porosity may play a different role than would be expected as porosity is expected to weaken a ceramic material instead of initially strengthening it as shown in this data. Data was gathered using conventional sintering and compared with the above-mentioned microwave sintering data.

## 1.2. Processing of Green Samples

Particle size of the starting powder was first reduced through grinding of the powder in a mortar and pestle. After failed attempts of producing green samples (unsintered) through isostatic pressing, Elmer's glue was incorporated as a binder (this was used instead of polyvinyl alcohol – a common binder). We found that using standard glue as a binder produced good quality samples from uniaxial pressing. One drop of glue (approximately 1 mg) to ten drops of water was used per gram of material. Once the mixture was completely dry, approximately ten drops of water were added to the mixture right before pressing. Green samples were made by uniaxially pressing regolith powder with a load of between 9340 and 10675 N (2100-2400 lbs) of force on a cross-section of 6 x 6 mm with lengths ranging from 12-35 mm giving a stress range between 260-295 MPa.

Later samples fabricated without binder were both conventionally sintered and microwave sintered at 1125 °C and 1150 °C in the microwave and 1100 °C, 1150 °C, and 1200 °C in a conventional furnace. Hold times at temperature for these samples were 30, 60, 90 and 120 minutes for the microwave heated samples and 120 minutes for all the conventionally sintered samples. The fracture toughness samples were heated at 1125 °C in a microwave furnace for 30 minutes and at 1100 °C for 2 hours in a conventional furnace.

## 1.3. Sintering of Asteroid Regolith

Green samples were sintered using from 125 watts to 1000 watts of microwave power in a Panasonic microwave oven at 2.45 GHz. Each sintering run consisted of placing three green samples on an aluminum oxide setter plate that was sprayed with boron nitride. The samples were then placed inside an insulation box made of Babcock and Wilcox insulation board (15C board) and placed inside the cavity of the microwave furnace. Zirconia beads were used to aid in the heating of the approximately 1 g samples. Zirconia couples well to 2.45 GHz radiation and was used because the samples weight of a few grams did not present a sufficient load to the output of the magnetron to cause efficient coupling to bring about sintering. Initially, larger bulk loads (50 to 100 g) of regolith were heated by themselves in the microwave field. A 1-inch in diameter hole was then cut into the side of the microwave as well as the adjacent alumina wall so that an infrared camera could determine the temperature of the samples. The microwave has the ability to change the power level in increments of 10% of maximum power, allowing for slow heating rates which prevents cracking and to prevent large amounts of porosity from forming within the sample. Sintering usually began at P4 (40% of 1250 watts) for 1 hour, and was then taken to the desired temperature using 750 watts of microwave power. Once the desired temperature was reached, the samples were held there for 15 minutes at temperature and then slowly cooled under microwave radiation at room temperature. Samples were also sintered in a conventional furnace at temperatures ranging from 1050 °C to 1250 °C in 50 °C increments. Samples sintered below 1200 °C were sintered for 6 hours at temperature and those samples sintered above 1200 °C were sintered for 2 hours. A second microwave furnace (BP-125 Microwave Research & Applications, Inc) was used to fabricate samples in a microwave environment. This furnace had better temperature control and was equipped with an internal temperature thermal probe to give an approximate temperature without using an IR camera. The temperature accuracy was given by the manufacturer to be ± 50 °C. All of the samples fabricated without a binder were fabricated using this microwave furnace.

## 1.4. Results and Discussion

Young's modulus of elasticity was also determined for both microwave and conventionally heated material. This data presented in Table 1 and Table 2. Values for the Young's modulus, *E*, were determined from the flexure strength data using the standard three-point flexural strength test using an Instron ElectroPuls E1000 testing device shown in Figure 1. The values for the Young's modulus for both the microwave and conventionally sintered material is shown in Figure 2.



Figure 1: Instron ElectroPuls E1000 used to determine flexure strength of asteroid regolith simulant.
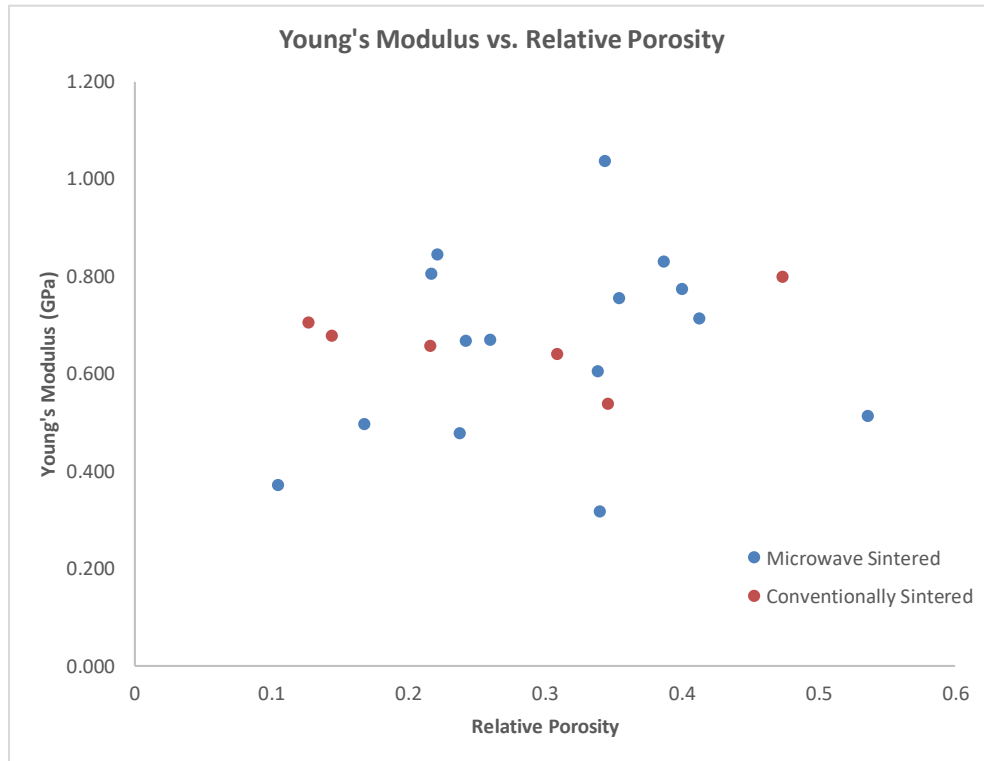
Figure 2: Young's modulus as determined from three-point flexure strength testing of microwave and conventionally sintered regolith simulant.

Table 1: Sample information for microwave sintered CI asteroid regolith simulant.

| | | | | Microwave Sintered | |
|---|---|---|---|---|---|
| Sample (Temperature-Number) | Density (g/cc) | Porosity (% Volume) | Flexure Strength (Mpa) | Young's Modulus (GPa) | Hardness (HV) |
| N-1125-M-1-15 | 2.895 | 0.105 | 14.868 | 0.370 | 298.55 |
| N-1125-M-2-15 | 2.66 | 0.34 | 16.571 | 0.316 | Not Measured |
| N-1125-M-3-15 | 2.587 | 0.413 | 27.550 | 0.714 | 335.35 |
| N-1150-M-15-1 | 2.758 | 0.242 | 21.672 | 0.668 | 355.1 |
| N-1150-M-15-2 | 2.74 | 0.26 | 29.491 | 0.669 | 280.4 |
| N-1175-M-1-15 | 2.762 | 0.238 | 11.231 | 0.478 | Not Measured |
| N-1175-M-2-15 | 2.661 | 0.339 | 20.823 | 0.605 | 238.9 |
| N-1175-M-3-15 | 2.832 | 0.168 | 10.589 | 0.496 | Not Measured |
| N-1200-M-1-20 | 2.464 | 0.536 | 21.065 | 0.513 | 359.75 |
| N-1200-M-1-30 | 2.783 | 0.217 | 33.750 | 0.805 | 348.4 |
| N-1225-M-1-15 | 2.779 | 0.221 | 32.162 | 0.845 | 344.15 |
| N-1250-M-1-15 | 2.613 | 0.387 | 34.175 | 0.831 | Not Measured |
| N-1275-M-2-15 | 2.646 | 0.354 | 35.309 | 0.754 | Not Measured |
| N-1275-M-3-15 | 2.656 | 0.344 | 43.492 | 1.036 | Not Measured |
| N-1300-M-1-15 | 2.6 | 0.4 | 31.598 | 0.773 | Not Measured |

Table 2: Sample information for microwave sintered CI asteroid regolith simulant.

| Conventionally Sintered | | | | | |
|---|---|---|---|---|---|
| Sample (Temperature-Number) | Density (g/cc) | Porosity (% Volume) | Flexure Strength (Mpa) | Young's Modulus (GPa) | Hardness (HV) |
| N-1225-C-1 | 2.784 | 0.216 | 33.505 | 0.658 | Not Measured |
| N-1225-C-2 | 2.873 | 0.127 | 25.208 | 0.705 | Not Measured |
| N-1225-C-3 | 2.856 | 0.144 | 20.771 | 0.677 | Not Measured |
| N-1275-C-2 | 2.691 | 0.309 | 21.891 | 0.640 | Not Measured |
| N-1275-C-3 | 2.654 | 0.346 | 18.028 | 0.539 | Not Measured |
| N-1300-C-3 | 2.526 | 0.474 | 32.422 | 0.799 | Not Measured |

Hardness values were determined for microwave sintered regolith in Figure 3 using a Vickers pyramid microhardness indenter using a Buehler Model 1600 hardness tester (Figure 4).
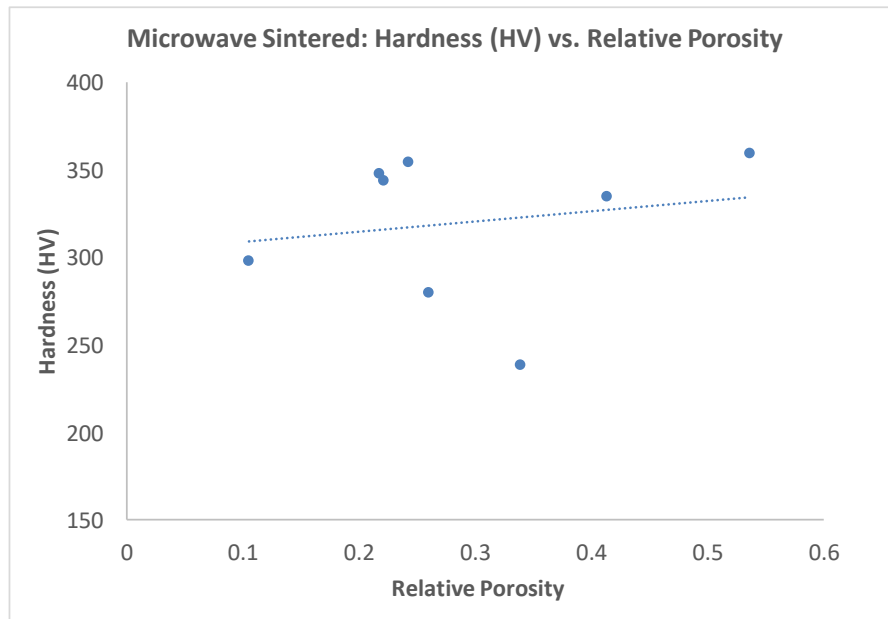


Figure 3: Hardness data for microwave sintered CI asteroid regolith simulant.

Figure 4: Buehler Model 1600 hardness tester with Vickers hardness indentation tip.

Thermal conductivity and thermal diffusivity was also determined for microwave sintered simulant regolith (1125 °C for 30 minutes) and was found to be approximately 0.62 ± 0.05 W/m-K and thermal diffusivity to be (on computer).

Lastly, thermal shock behavior was investigated for both conventional and microwave sintered regolith simulant. This data is presented in Table 3 and Figure 5. As seen in the figure, it suggests that thermal shock behavior for conventionally sintered material is what is normally observed (approximately 150 °C ΔT). While this is a little lower than expected values for most ceramic materials using this method (300 150 °C ΔT) the behavior is fairly normal. The thermal shock behavior observed for the microwave sintered material is also similar to that seen by one of the authors (T. Meek) in other ceramic materials investigations (reference). For microwave heated material, the thermal shock behavior increases to well above the normal thermal behavior (approximately 350 °C ΔT). The thermal shock experiments were performed with a custom vertical tube furnace. The samples were heated to a predetermined value and then dropped into a beaker of water with a known temperature (100 °C) to attain a known ΔT value. This furnace is shown in Figure 6.

Table 3: Flexure strength and thermal shock data for microwave and conventional samples.

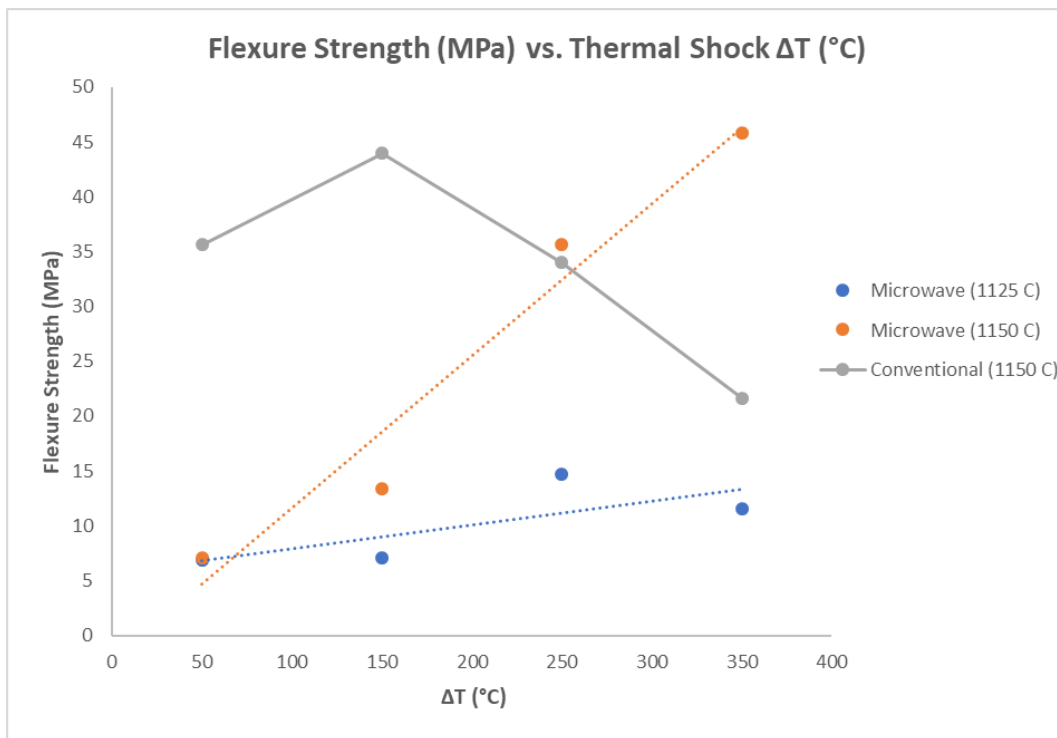| Sample ID | Flexure Strength (MPa) | ΔT (°C) |
|---|---|---|
| **Microwave (1125 °C)** | | |
| **M-1125-30-4** | 5.494 | 50 |
| **M-1125-60-4** | 7.105 | 150 |
| **M-1125-90-1** | 14.651 | 250 |
| **M-1125-120-3** | 11.571 | 350 |
| **Microwave (1150 °C)** | | |
| **M-1150-90-1** | 7.028 | 50 |
| **M-1150-90-2** | 4.945 | 150 |
| **M-1150-60-1** | 29.354 | 250 |
| **M-1150-120-5** | 31.019 | 350 |
| **Conventional (1150 °C)** | | |
| **C-1150-120-1** | 35.604 | 50 |
| **C-1150-120-2** | 43.974 | 150 |
| **C-1150-120-3** | 33.995 | 250 |
| **C-1150-120-4** | 21.639 | 350 |



Figure 5: Flexure strength as function of thermal shock temperature change for microwave and conventionally sintered samples.

Figure 6: Vertical tube furnace configuration used to determine thermal shock temperature change for asteroid regolith simulant.

**Mechanical Properties**

The modulus of elasticity, flexure strength, and hardness were all plotted as a function of porosity. Porosity was calculated by comparing the known density to the maximum density of the simulant. The maximum density of the simulant was experimentally determined by completely melting a sample under microwave radiation at a temperature of 1429 °C since there is no literature value available. A density of 2.918 g/cc was measured. Data were also obtained on fracture toughness for both microwave and conventionally heated samples. An average value for the fracture toughness of mcirowave heated samples was 0.67 MPa√m (roughly comparable to concrete) and conventionally heated samples was 0.31 MPa√m. All of thi data is shown in Table 4. Data for fracture toughness was obtained using a Charpy testing instrument to determine sample break energy which was converted to fracture toughness, $K_Q$.

Table 4: Fracture toughness for microwave and conventionally sintered asteroid regolith simulant.

| Sintering Condition (C/M-Temp-#) | Crack Length (mm) | Fracture Toughness (MPaVm) |
|---|---|---|
| *Conventional (=C)* | | |
| C-1100-1 | 4.8 | FAILED |
| C-1100-2 | 4.8 | 0.264 |
| C-1100-3 | 4.8 | 0.365 |
| C-1100-4 | 4.8 | FAILED |
| *Microwave (=M)* | | |
| M-1125-1 | 4.7 | 0.692 |
| M-1125-2 | 4.9 | 0.709 |
| M-1125-3 | 4.9 | 0.541 |
| M-1125-4 | 4.8 | 0.753 |

# 3. Analysis of Aerocapture Effectiveness

## 3.1. Aeocapture Modeling

Aerocapture utilizes drag from passage of the returning spacecraft through the Earth's upper atmosphere to shed energy. Enough energy must be shed that the spacecraft is captured into Earth orbit during a single pass; otherwise it will sail back out into heliocentric space. Thus aerocapture is distinct from aerobraking, which is employed after a spacecraft is already captured into orbit at the destination planet, usually propulsively, in order to lower the initially high apoapse. Aerobraking can be arbitrarily gentle, at the expense of extended mission time, since there is no risk of escape of the spacecraft back to heliocentric space. It has been used several times with spacecraft at Venus and Mars after initial propulsive capture at those planets. These spacecraft are oriented during periapse passages so that their solar panels maximize the effective area for drag interaction. Since solar panels are not very robust structures, great care must be taken that aerodynamic and thermal stresses not exceed fairly modest limits, and that means the aerobraking phase of the mission is broken into many periapse passages for completion.

The much greater stresses imposed by aerocapture, though, means that a heat shield, or aeroshell, is required. Such an aeroshell can be manufactured on Earth, transported into space and hence to the asteroid target, and then back to Earth for its utilization. Carrying this large mass as a dead weight for most of the mission will seriously limit any advantage that aerocapture can provide. It will limit the amount of resources that can returned and/or limit the number of asteroids that can be accessed. If, however, the aeroshell can be manufactured at the asteroid, from the resources of the asteroid, then

most of these limitations will be avoided. In this study we seek to develop microwave-sintering technology that can create a heat shield from the regolith at the target asteroid.  A great deal of velocity can be removed with aerocapture, widening the population of accessible NEAs by tens of times compared to propulsive capture, or propulsive capture aided by lunar swingby.  However, fabricating a heat shield in space would be a new innovation.

During this study the software tool GMAT (General Mission Analysis Tool) was used to model the dynamics of the aerocapture pass.  The parameters and conditions shown in Fig. 7 were arrived at after considerable iteration.  The spacecraft total mass was held fixed at 100 tonnes during this exercise, though it is recognized that this much mass may end up being divided into multiple spacecraft upon application of optimality trade studies and/or practical limitations.  In general, it is desired to accommodate the maximum incoming energy (C3) since the higher the energy that can be captured from, the more asteroids become accessible via aerocapture.  This goal works against other goals of the scenario; one being to minimize the drag area of the aeroshell, since greater area likely will correspond to greater aeroshell mass as well as possible aero-stability issues.  Aeroshell mass, as a proportion of the total returned mass, may be less of a negative driver than it first may seem as long as it's produced at the asteroid.  That's because the aeroshell material itself will be a valuable and sellable resource.  Another goal is to keep the perigee of the aerocapture pass as high as possible, since lower altitudes will subject the spacecraft to greater mechanical and thermal stresses, and the effect of trajectory errors at low altitude will be greater.  There may also be political considerations that will restrict the perigee to be above a certain altitude.  In any case, there is likely enough freedom in selecting the time of the aerocapture pass that the perigee can be targeted to occur over ocean rather than land and populated areas.

In GMAT the input parameters of Drag Area and projected Perigee Altitude were varied until a desired Post-Aeropass C3 (energy) was achieved.  Aerocapture can be used to achieve a strongly captured (strongly negative C3) Earth orbit, which likely will be closer to the desired destination orbit.  But this would be done at the expense of limiting the incoming C3, and thus the number of NEAs accessible, with other aerocapture parameters being the same.  Going the other way, a weakly captured (marginally negative C3) Earth orbit would maximize the incoming C3, and thus expand the number of NEAs accessible via aerocapture.  But such a weakly captured orbit would have a very high apogee and period.  Solar and lunar perturbation could then have the effect of causing the "captured" payload to escape into heliocentric space or, depending on geometry, the perturbations could have the beneficial effect of reducing C3.  Either way, mission operations would become much more complex, and/or the mission timeline greatly extended (potentially by months) due to the long period of the post-aerocapture orbit.  For now, a conservative approach was taken with a "moderately" negative C3 range of -1.5 to -2.0 $km^2/s^2$ being targeted.  For the scenario parameters presented, a post-aerocapture C3 of -1.6 was achieved, with a period of 14.2 days.

For the scenario depicted in Fig. 7 a prograde, equatorial approach to Earth was modeled.  This was because nearly any desired post-capture orbit will be prograde and it would be difficult, operationally and/or from propellant usage, to go from retrograde to prograde.  Prograde aerocapture is, however,

slightly less efficient for capture than retrograde since the spacecraft's velocity, relative to the atmosphere, is lower resulting in lower dynamic pressure at any given altitude. The penalty was found to be small, however, with equatorial retrograde aerocapture requiring perigee about 1 km lower than for prograde equatorial, all other parameters being equal. Actual aerocapture trajectories will be from a wide variety of inclinations, so the scenario modeled here represents the worst-case for this consideration.
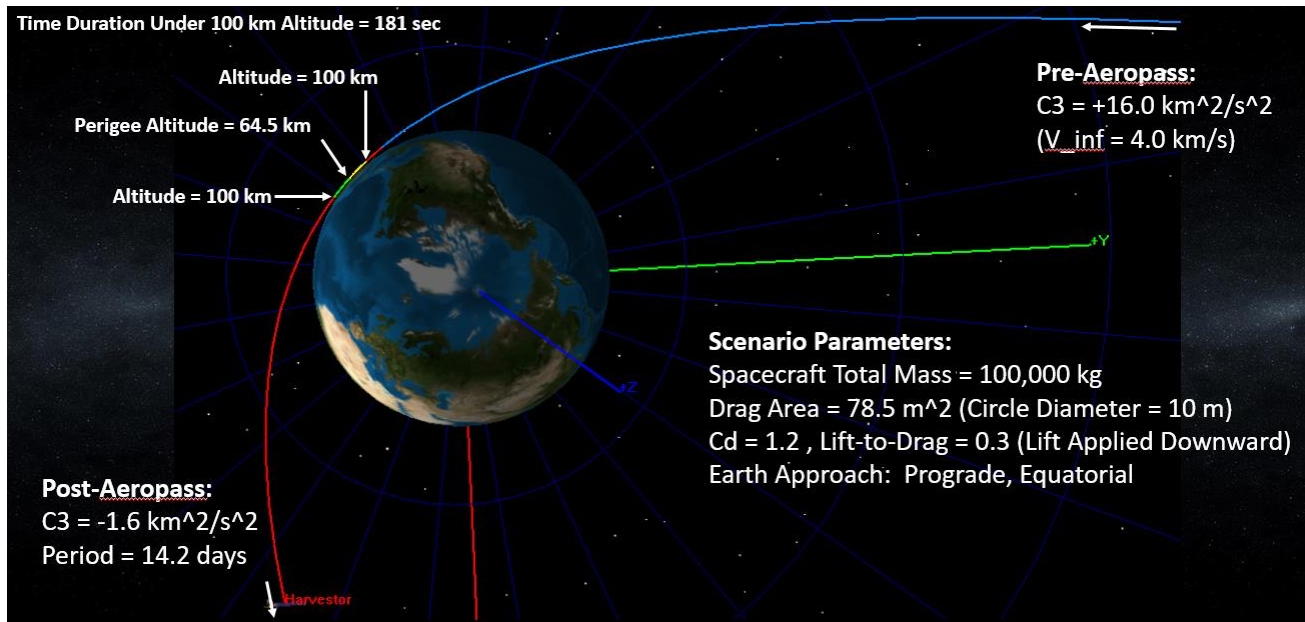


Figure 7: Aerocapture to HEEO, Modeled Using GMAT

The GMAT scenario depicted in Fig. 7 utilizes a MSISE90 atmospheric drag model. A Cd (coefficient of drag) of 1.2 was selected as representative of this altitude and dynamic environment. Aerocapture can be achieved without any lift force, in which case the drag force is aligned with the velocity of the spacecraft (i.e., in-track) through the atmosphere. However, lift applied downward (toward Earth) has a beneficial effect. It effectively holds the spacecraft at lower altitudes, where energy is removed at a greater rate, for a longer period of time, and without the peak loading needing to be as high. This allows the drag area (and thus aeroshell size and mass) to be smaller and/or the perigee altitude to be higher than otherwise. This benefit increases as Lift-to-Drag ratio increases. Here, a ratio of 0.3 was used, as a practical upper limit for the relatively simple aeroshell shapes that will likely be manufacturable at the asteroid. The limit on Lift-to-Drag ratio will be examined more closely during Phase II.

Figure 8 shows a timeline of drag and lift force on the spacecraft during the period that it is below 100 km altitude, where such forces become significant. The peak load, near perigee, is about 1.1 g. This is well within the strength limits revealed thus far by testing of microwave-sintered asteroid simulant, as shown in this study. One can subject the spacecraft to greater loads, closer to the materials limit, by using a smaller drag area which would have the beneficial effect of allowing a smaller and lighter

aeroshell.  But the compensation would require a deeper dive into the atmosphere to effect the same energy loss, and that would incur the risks described above.  The current scenario, we believe, strikes a reasonable balance between these parameters.  But we will explore the trade-offs more deeply during Phase II, including reasonable margins on the load limits as the strength limits and variability of microwave-sintered regolith become more firmly established.
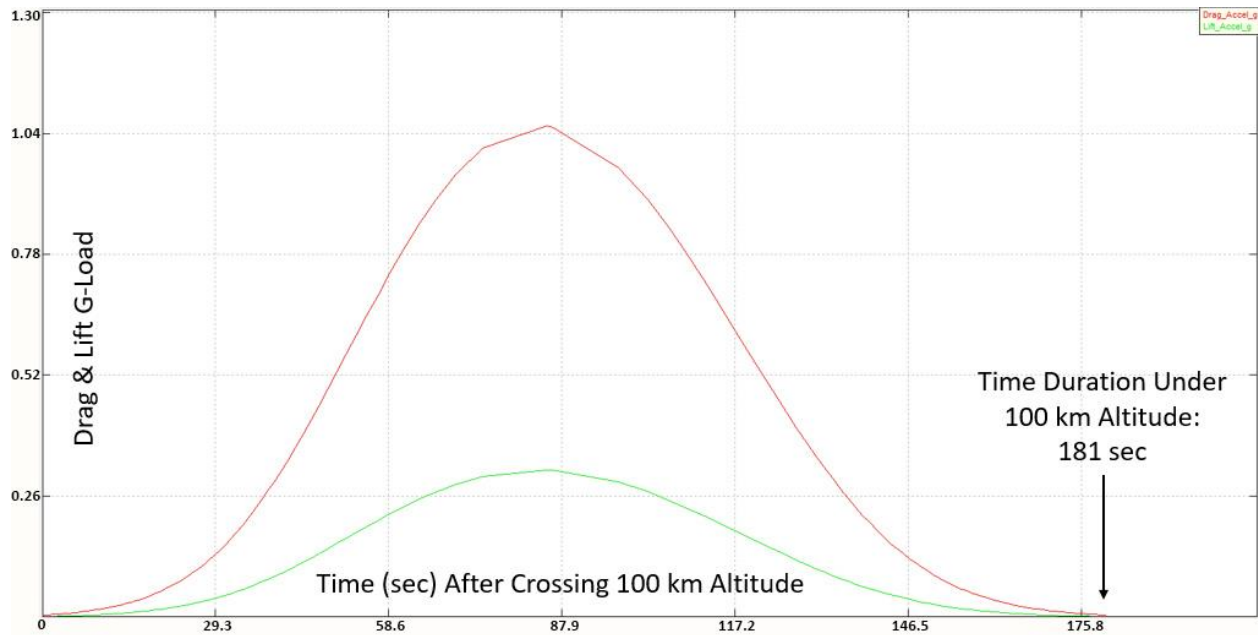


Figure 8: G-Loading During Aerocapture Pass, Modeled Using GMAT

The parameters of Cd = 1.2, and Lift-to-Drag = 0.3 were used after discussion of the issues with Terminal Velocity Aerospace (TVA). TVA will be a partner with DSI for the Phase II proposal of this study. TVA also conducted an independent analysis of the aerocapture, using the same parameters as did DSI. For this analysis they used their proprietary trajectory optimization software, QuickShot. The results between the two modeling tools were very similar, with perigee altitudes 100 m apart (64.5 km in GMAT vs. 64.4 km in QuickShot). Various profile plots through the aerocapture pass also tracked each other well between the two modeling tools (Figure 9). Interestingly, in QuickShot the lift force being applied strictly downward was a result of satisfying an optimality condition, that the perigee altitude be maximized, whereas the application of downward lift was assumed in GMAT.  GMAT does not have a built-in capability to model lift force.  But it was emulated by modeling a thruster whose thrust level was reset at frequent altitude intervals through the atmospheric passage, in order to maintain the desired ratio of this lift force (downward) to the drag force during the changing atmospheric conditions.

The correctness of aerocapture trajectory modeling, using GMAT, was supported by the independent analysis by TVA using QuickShot.  Some basic physical characteristics of the capture scenario, such as the g-load history shown in Fig. 8, and energy-loss history from the C3-reduction timeline, can be inferred using this tool.  But the aeroshell properties are represented in GMAT only through the simple

parameters of total mass, drag area, and Cd.  TVA has the tools and expertise to go beyond these limitations, and incorporate the physical properties of the microwave-sintered regolith meaningfully into the analysis.  Important considerations including aerodynamic stability and mode of heat dissipation (radiation, ablation, conduction) will be addressed by TVA during Phase II.  An indication of TVA's extended capabilities are indicated in Figure 10, showing heat rate and dynamic pressure timelines.
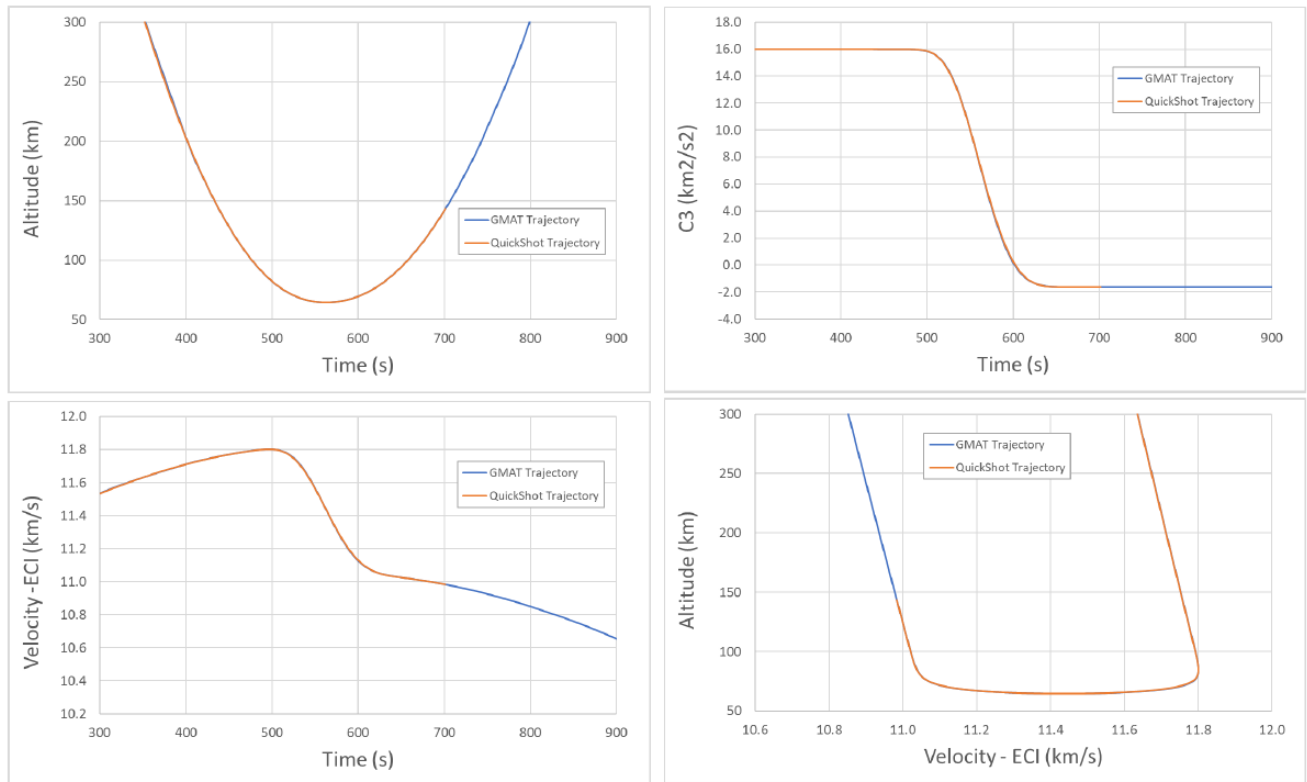


Figure 9: Baseline Trajectory Results, from TVA, Comparing GMAT and QuickShot Trajectories
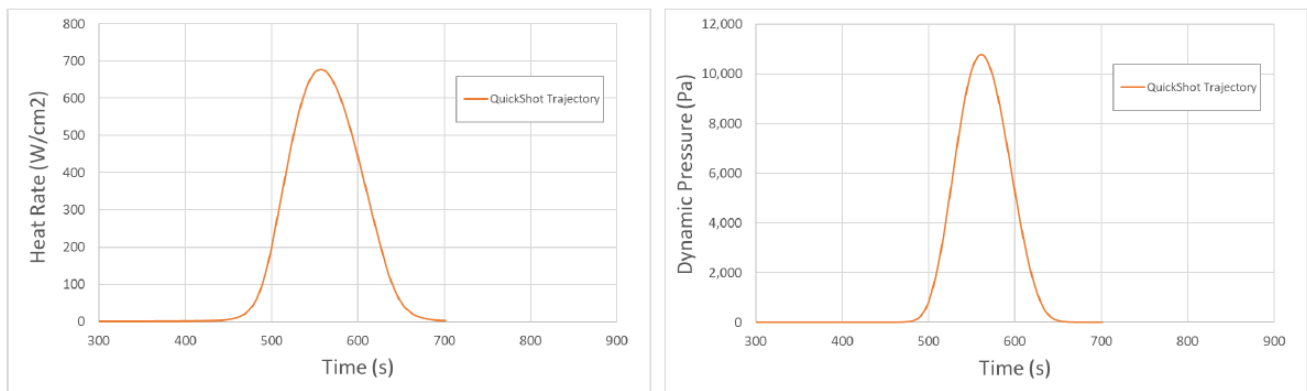


Figure 10: Baseline Trajectory Results, from TVA, Showing Thermal and Dynamic Loading History

## 3.2. Expanded NEA Accessibility via Aerocapture

NEA accessibility expansion was addressed from an overall NEA population viewpoint using queries to the JPL Small-Body Database Search Engine, with results shown in Table 5.  Any given C3 value for a spacecraft incoming to the aerocapture corresponds to a maximum aphelion distance (Q), if the perihelion distance (q) is assumed to be close to Earth's distance (q ~= 1 AU).  A maneuver at aphelion, here fixed at 500 m/s, was applied to expand the range of q's accessible.  Such a maneuver will favor higher energy (greater Q), expanding the range of q that is within range (as seen in Table 5).  That, in turn, expands NEA accessibility for higher incoming C3, more than just the increase in Q would yield.  Using these distance limits (Q & q) as search constraints within the JPL SBDB Search Engine yields the number of NEAs (and their identities) for each value of incoming C3.  Although the majority of NEAs identified this way are unlikely to be viable mission candidates for numerous reasons, the column labeled "Access Expansion" shows the <u>ratio</u> of the NEA numbers, relative to the lowest C3 value, and should be an indicator of the resulting accessibility expansion.  The validity of this ratio comparison assumption depends on the proportion of mission-viable vs. total NEAs being constant across the C3 range examined (TBC).  The comparison with lunar swing-by capture (first row) is, likely, unfair to aerocapture since NEAs compatible with lunar swing-by capture have been shown to be much more limited by their initial heliocentric inclination than are those candidates for aerocapture.

NEA accessibility expansion here is posed purely in terms of orbital parameters, which favors aerocapture over propulsive capture as one goes to higher incoming C3.  But the NEAs accessible at higher C3 are <u>also</u> likely to be richer in volatile resources since they spend much less time in the higher temperature environment closer to the Sun.  NEAs in orbits very close to that of Earth, including most of the Atens, are especially likely to be depleted in desirable resources.  Such NEAs are also at the limit of what may be captured via lunar swingby, suggesting this method cannot be relied upon for retrieval of economically significant resources except, perhaps, as a supplement to aero or propulsive capture.  Spectral characterization of NEAs is sparse, and searchable databases such as the JPL SBDB Engine, may be especially slow to incorporate such data as that there is.  Accessibility expansion for <u>resource-rich NEAs</u> is thus likely to be much more dramatic than the numbers shown in Table 5 but, at present, data are not available to confirm that assertion.

Lunar swingby capture was equivalent to aerocapture at the lowest energy level (C3=2.56) in terms of NEAs accessible. For each incoming C3 value the non-payload portion of the mass (propulsion, power, structure, tankage, etc.) was accounted for, the propellant used was calculated, and hence the percent of payload mass remaining after asteroid departure, Earth-orbit capture, and perigee raise.  The post-capture energy was assumed to be C3 = -1.5 $km^2/s^2$, the aerocapture perigee at 70 km, and the propulsive maneuver executed impulsively at 100 km altitude.  A post-capture apogee maneuver is also executed to raise perigee from these altitudes to 400 km.

The four right-most columns in Table 5 show the relative payload mass reduction for aero vs. propulsive capture, at two $I_{sp}$ values (200s representing direct use of NEA water in an electro-thermal or solar thermal propulsion unit, and 300s representing a non-cryogenic bipropellant system that would involve delivering more mass to the NEA to accommodate more on-site processing steps).  With aerocapture

the amount of payload returned is constant across the range of incoming C3.  The asteroid-departure ΔV, and thus propellant used, is constant, no propellant is used during aerocapture, and the perigee-raise maneuver is thus also constant. It is likely that the aeroshell will need to be "beefier" at higher incoming C3.  But since the aeroshell material, as well as the volatile payload, is considered sellable payload, the payload proportion simply shifts more toward aeroshell from volatiles without changing this calculation.

By contrast, with propulsive capture the percentage of the spacecraft mass captured drops steeply with higher incoming C3.  This likely offsets the benefit of expanded NEA access and favors the aerocapture scenario.

Table 5: NEA Accessibility Expansion over Range of Incoming C3 (Database Search)

| Incoming V_infinity | Incoming C3* | # NEAs in Data-base Search | Access Expansion vs. Lunar Swingby | Percent of Payload Remaining After Capture | | | |
|---|---|---|---|---|---|---|---|
| | | | | w Aerocapture (Preliminary) | | w Propulsive Capture (Preliminary) | |
| km/s | km$^2$/s$^2$ | | | Isp=200s | Isp=300s | Isp=200s | Isp=300s |
| 1.6 | 2.56 | 239 | -- | 74% | 82% | 64% | 75% |
| 2.0 | 4.00 | 363 | 52% | 74% | 82% | 61% | 73% |
| 3.0 | 9.00 | 821 | 244% | 74% | 82% | 52% | 66% |
| 4.0 | 16.00 | 1,533 | 541% | 74% | 82% | 41% | 57% |
| 4.5 | 20.25 | 1,963 | 721% | 74% | 82% | 36% | 52% |
| 5.0 | 25.00 | 2,463 | 931% | 74% | 82% | 30% | 47% |

*Max aphelion distance (Q) increased from 1.248 to 2.144 AU, and perihelion range (q) increased from 0.931:1.075 to 0.913:1.095 AU as Incoming C3 increased over the range shown.

The results in Table 5 are preliminary because they depend on very approximate values for key variables that were estimated during the short Phase I study period.  Key factors with imprecise values are the non-payload masses required by the two types of Earth return.  Phase II will seek higher validity inputs for how these masses vary between the two types of Earth returns, especially the two propulsion systems.

In Phase II we will also consider returning to Earth orbit, for use on succeeding missions, equipment that is used at the asteroid for volatile extraction, propellant production, and aeroshell manufacture.  The benefit of reusing such equipment as much as possible is obvious, but its return to Earth orbit is penalized by the rocket equation, increased operational complexity and, possibly, by limits to equipment lifetime that would reduce the reliability of succeeding missions.  Table 5 does not model return to Earth orbit of such equipment.  If it did, it's expected that return to Earth orbit of propellant extraction and production equipment would increase further the favorability, especially at higher incoming C3 levels, of aerocapture over propulsive capture.  That's because, for a given spacecraft mass returning to Earth, the propulsive capture scenario requires and uses more propellant production, and

the equipment for that will be correspondingly heavier.  On the other hand, return to Earth orbit of the aeroshell manufacture equipment penalizes the aerocapture scenario since that equipment isn't needed for the propulsive capture scenario.

# 4. Conclusions

Phase I research showed that simulated asteroid regolith could be microwave sintered into blocks that were sufficiently strong to withstand the stresses predicted by aerobraking simulations.  The energy required was substantially less than if conventional sintering were used.  Phase I aerocapture analysis also found that significant incoming relative velocity could be cancelled by a 10-meter aeroshell if aimed at a perigee of 64.5 km.

However, the microwave sintering produced samples with relatively wide strength ranges that need to be narrowed in Phase II.  In addition, the feasibility of producing a 10-meter diameter aeroshell as one unitary object is unknown, and the alternative of producing multiple plates that are sintered together to form the overall shell is seen to be an important research topic for Phase II.

In addition, the modeling tools available in Phase I for aerocapture were too basic to answer important questions, such as how thick the aeroshell should be, what shape would be most effective, and how much of the return payload mass would be required by the aeroshell and how much would be available for the volatiles.  These issues will be addressed in Phase II research.